LA-UR-23-25023
Accepted Manuscript

Passive methods for spent fuel characterisation at the Finnish geological repository

Tobin, Stephen Joseph; Dendooven, Peter; Virta, Riina; Tupasela, Topi; Moring, Mikael; Bubba, T.A.; Siltanen, S.; Hahkonen, T.; Makkonen, I.; Laassiri, M.; Andersson, Peter; Honkamaa, Tapani

Provided by the author(s) and the Los Alamos National Laboratory (2025-08-11).

To be published in: Il Nuovo Cimento C

DOI to publisher's version: 10.1393/ncc/i2023-23047-4

Permalink to record:
https://permalink.lanl.gov/object/view?what=info:lanl-repo/lareport/LA-UR-23-25023

Los Alamos NATIONAL LABORATORY

NNSA National Nuclear Security Administration

Los Alamos National Laboratory, an affirmative action/equal opportunity employer, is operated by Triad National Security, LLC for the National Nuclear Security Administration of U.S. Department of Energy under contract 89233218CNA000001. By approving this article, the publisher recognizes that the U.S. Government retains nonexclusive, royalty-free license to publish or reproduce the published form of this contribution, or to allow others to do so, for U.S. Government purposes. Los Alamos National Laboratory requests that the publisher identify this article as work performed under the auspices of the U.S. Department of Energy. Los Alamos National Laboratory strongly supports academic freedom and a researcher's right to publish; as an institution, however, the Laboratory does not endorse the viewpoint of a publication or guarantee its technical correctness.

IL NUOVO CIMENTO **46 C** (2023) 47
DOI 10.1393/ncc/i2023-23047-4

COLLOQUIA: SOGIN 2023

Passive methods for spent fuel characterisation at the Finnish geological repository

P. DENDOOVEN(1), R. VIRTA(1)(2), T. TUPASELA(2), S. J. TOBIN(3), M. MORING(2), T. A. BUBBA(4), S. SILTANEN(5), T. KÄHKÖNEN(6), I. MAKKONEN(7), M. LAASSIRI(1), P. ANDERSSON(8) and T. HONKAMAA(2)

(1) *Helsinki Institute of Physics, University of Helsinki - Helsinki, Finland*
(2) *Radiation and Nuclear Safety Authority (STUK) - Vantaa, Finland*
(3) *Los Alamos National Laboratory - Los Alamos, NM, USA*
(4) *Department of Mathematical Sciences, University of Bath - Bath, UK*
(5) *Department of Mathematics and Statistics, University of Helsinki - Helsinki, Finland*
(6) *VTT Technical Research Centre of Finland - Espoo, Finland*
(7) *Department of Physics, University of Helsinki - Helsinki, Finland*
(8) *Department of Physics and Astronomy, Uppsala University - Uppsala, Sweden*

received 7 March 2023

Summary. — Development of the Passive Gamma Emission Tomography (PGET) and Passive Neutron Albedo Reactivity (PNAR) methods in the context of the Finnish geological repository for spent nuclear fuel has shown that they provide, for BWR fuel assemblies, the comprehensive verification needed to meet the nuclear safeguards objectives of the repository. The principles of the PGET and PNAR methods and the design and operation of the respective instruments are presented. A few results from measurements at the spent fuel storage pools at the Finnish nuclear power plants are discussed. The directions of ongoing and future developments are indicated.

1. – Introduction: safeguards for the Finnish geological repository for spent nuclear fuel

Finland will be the first country in the world to start disposal of its spent nuclear fuel in a deep underground geological repository. Filling of the ONKALO repository [1], on the West coast of Finland next to the Olkiluoto nuclear power plant, is planned to start in 2025. Disposal canisters will be filled with 12 fuel assemblies at the encapsulation plant which sits on top of the repository. Canisters will be placed in vertical holes at a depth of about 430 m. The spent fuel is shielded by several barriers: the fuel rod cladding, the canister, the bentonite fill of the vertical holes, the tunnel backfill and the bedrock in which the repository has been dug.

Creative Commons Attribution 4.0 License (https://creativecommons.org/licenses/by/4.0)

The Finnish Radiation and Nuclear Safety Authority (STUK) has developed a national safeguards concept for the ONKALO repository. This concept requires that all fuel that goes down for disposal is accurately verified, that conclusions are transparently and reliably drawn by the inspectorates and that the results are well-documented for future generations. In this context, all spent fuel assemblies will be non-destructively characterised at their interim storage pool before being transported to the encapsulation plant. Passive Gamma Emission Tomography (PGET) will be used to verify the presence of fuel at the level of a single rod, while a Passive Neutron Albedo Reactivity (PNAR) measurement will indicate the presence of fissile material. These measurement outcomes will be combined in a final safeguards assessment.

In this article, the PGET and PNAR methods and devices are described and a selection of results from spent fuel measurements at the Finnish nuclear power plants (NPP) in Olkiluoto and Loviisa are presented. Some ongoing and future research and developments are listed.

2. – Passive Gamma Emission Tomography (PGET)

2˙1. *The PGET principle.* – An introduction to gamma ray emission imaging was recently published by Dendooven and Bubba [2]. In gamma emission tomography, n-dimensional radiographs of the emitted gamma rays are measured from different viewing angles (usually over a full 360 degree rotation). An image reconstruction algorithm transforms the radiographs vs. angle into an (n+1)-dimensional image of the object.

A fuel assembly is an array of about 50 to 300 fuel rods (2 to 4 m long), and a diameter of 10 to 20 cm. Gamma emission tomography for safeguards purposes creates 2D transaxial images by rotating a 1D gamma camera in the transaxial plane around a fuel assembly. Investigation of the fuel assembly in the axial direction requires tomography at different axial positions.

2˙2. *The PGET instrument design and data acquisition.* – The development of a PGET instrument for spent fuel inspection started in the 1980's under the guidance and support of the IAEA. A prototype device was designed and constructed and characterised with various types of spent fuel assemblies, and verified for spent fuel inspections by IAEA at the end of 2017 [3-5], see fig. 1.

The PGET instrument is toroidal in shape. The fuel assembly under investigation is lowered in the central hole of the torus. Two gamma cameras inside the toroid rotate around the fuel assembly. As measurements are performed under water, the toroid is water-tight and pressure resistant, with data, power and communication cables running to the instrument operation system installed at the side of the spent fuel storage pool.

Each gamma camera consists of a linear array of collimator slits, with a small cadmium zinc telluride (CZT) detector ($3.5\times3.5\times1.75$ mm^3) right behind each slit. The slits are 1.5 mm wide and have a pitch of 4 mm. The tungsten collimator is 100 mm thick. The slits are conical in the vertical direction (this is the axial direction of the fuel assembly), tapering down from 70 mm at the front to 5 mm at the back of the collimator. As such, the gamma camera looks at an axial section of the fuel assembly of about 20 cm. The two gamma cameras are offset by 2 mm; interleaving the data results in 1D radiographs (profiles) with 2 mm spatial steps.

During tomographic data acquisition, the gamma cameras are rotated at constant speed. The user defines the number of angular bins and the measurement time per angular bin. Typically, 360 angular bins (so 1 degree per bin) and 800 ms per bin are

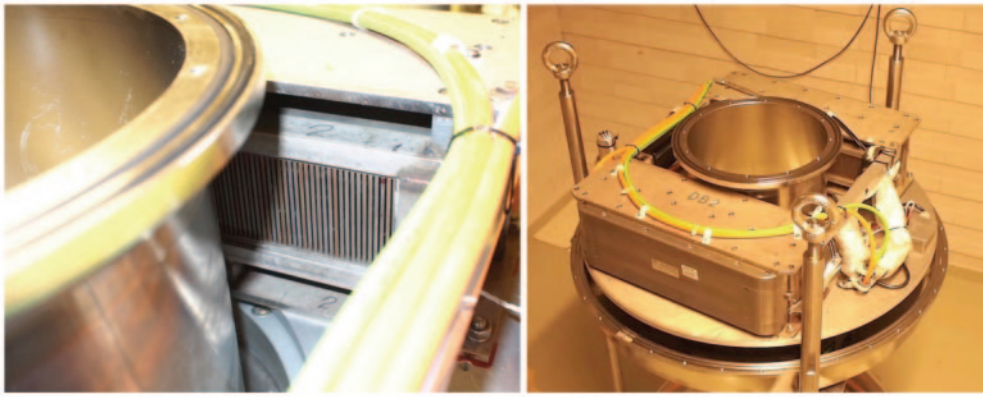

Fig. 1. – The inside of the PGET instrument is visible with the water-tight cover removed. Left: view of the front face of the collimator slits. Right: A 1D gamma camera is positioned before and behind the central hole into which a spent fuel assembly to be investigated is lowered. The gamma cameras are mounted on a common platform which rotates around the central hole for tomographic imaging.

used. The basic data collected during tomographic data acquisition are the number of counts above 4 user-defined energy thresholds for each angular bin. Differences of these numbers of counts give the number of counts in energy windows. This is the raw data used for image reconstruction. In recent measurements, the following energy windows were commonly used: 400-600 keV, 600-650 keV, 650-700 keV and 700-3000 keV (3000 keV being the highest energy that can be registered).

2˙3. *Tomographic image reconstruction and image analysis.* – In imaging for safeguards purposes, it is essential that no (assumed) prior information concerning the fuel assembly is used. We have therefore developed a 2-step image reconstruction method [2, 7, 8]. In the first step, a filtered back-projection (FBP) image reconstruction, a method which does not use any prior information, is performed. The resulting rather poor quality image allows to determine the fuel assembly type and thus its geometric layout. In a second step, the final image is obtained via iterative reconstruction using the fuel assembly geometry determined in the first step as prior. Images looking like such an assembly are thus favoured in the iterative reconstruction. Nuclear fuel is highly attenuating for the gamma rays emitted by fission products. Correctly imaging the (relative) gamma activity throughout a fuel assembly thus requires taking attenuation into account. As there is no practical way of obtaining independent attenuation information, we have developed an iterative image reconstruction method in which activity and attenuation images are reconstructed simultaneously, being treated mathematically on equal footing. Most often, 120 equidistant angular bins out of the 360 acquired are used for image reconstruction as this was found to give the highest quality images.

The outcome of a PGET investigation is illustrated in fig. 2 for a BWR AA-8×8 assembly. Shown are the results from the 650-700 keV energy window containing the photopeak of the 662 keV gamma ray from ^{137}Cs. From the activity and attenuation images generated by the iterative reconstruction algorithm, the values averaged over the area of a fuel rod for each fuel assembly array location are calculated. The average

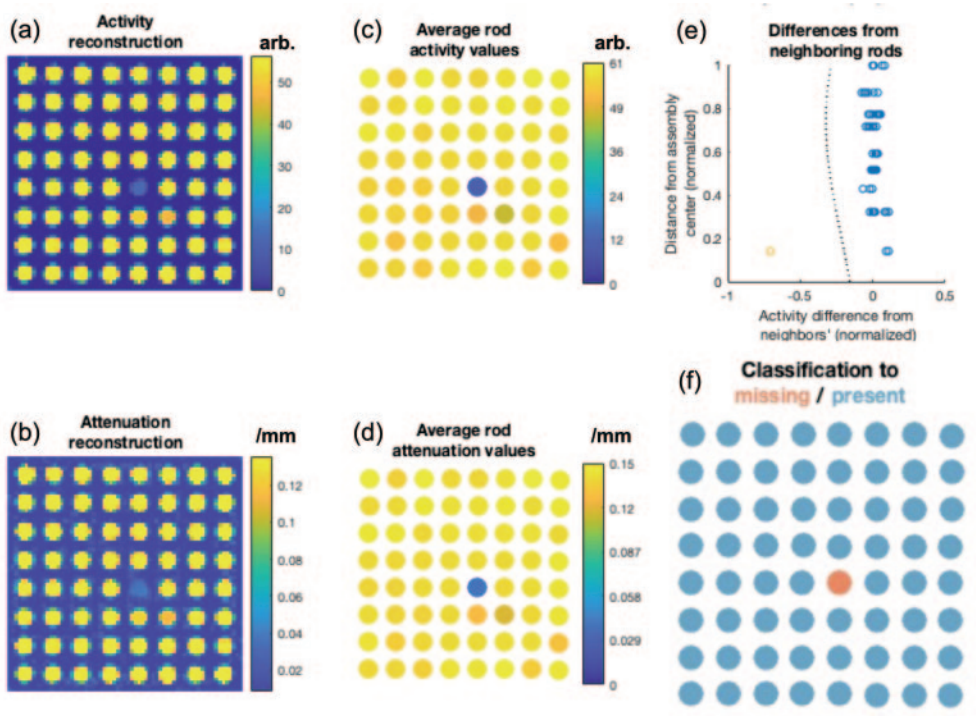

Fig. 2. – PGET images and classification of fuel assembly array locations for a BWR AA-8×8 assembly. This assembly is an 8×8 array of fuel rods with 1 rod missing. The reconstructed activity and attenuation images are show in (a) and (b). Their values averaged over the area of a fuel rod are given in (c) and (d). Figure (e) illustrates the classification method, with the dotted line showing the classification border. Figure (f) shows the final "traffic light" style image indicating whether fuel rods are present or missing. See the text and [7] for a detailed explanation.

activity values are used for classifying each fuel assembly array location. Presently, two classes are being considered: a fuel rod either being present or not being present (in which case there is water). For classification, the difference between the activity of each fuel assembly array location and the average of its neighbours is plotted versus distance to the centre of the fuel assembly. A support vector machine technique using images from a variety of fuel assemblies was used to define a classification border: fuel assembly array locations to the right of this border are classified as containing a fuel rod, whereas fuel assembly array locations to the left of this border are classified as missing a fuel rod. This classification results in a final "traffic light" type of image showing fuel rods being present or missing. In this example, the fuel rod missing by design of the AA-8×8 assembly and the 63 present fuel rods are very clearly identified.

2˙4. *A few results from PGET measurements at the Finnish NPPs.* –

2˙4.1. Energy windows. Figure 3 shows the activity images of the same fuel assembly as in fig. 2 for the 4 commonly used energy windows. The water position is best visible in the 650-700 keV and 700-3000 keV energy windows because these contain the main

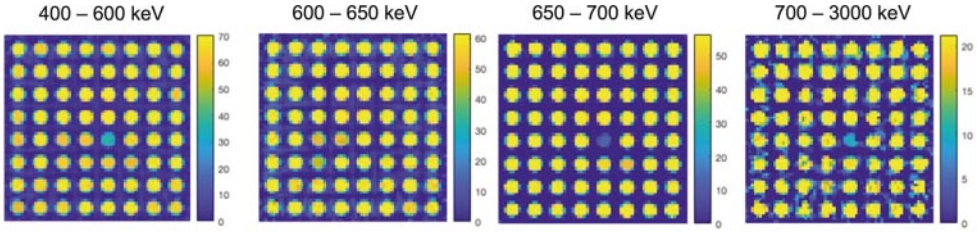

Fig. 3. – PGET activity images of the BWR AA-8×8 fuel assembly also shown in fig. 2 for the 4 commonly used energy windows. The water position is best visible in the 650-700 keV and 700-3000 keV windows, clearly visible in the 400-600 keV window, and not visible in the 600-650 keV window. See the text and [6] for a detailed explanation.

photopeaks at 662 keV for ^{137}Cs and at 1274 keV for ^{154}Eu. A gamma ray detected in a photopeak has not scattered before reaching the detector. It thus contains perfect directional information and maximum imaging information. The image from the 700-3000 keV energy window is of poorer quality, showing "speckle effects" due to the low number of counts. The 600-650 keV energy window does not reveal the water position at all. The reason is that, considering the largely dominating emission of 662 keV gamma rays from ^{137}Cs, the 600-650 keV window only contains gamma rays that scattered before reaching the detector. By scattering, these have lost their directional information and thus carry very poor imaging information. Perhaps surprisingly at first sight, the 400-600 keV window shows the water position, but somewhat less clearly than the windows containing the photopeaks. The reason is that this window contains the Compton edge of the 662 keV gamma ray, located at 478 keV. The Compton edge originates from the backscattering of full-energy gamma rays; thus representing gamma rays that hit the detector without scattering, containing perfect directional information and providing maximum imaging information.

The conclusion is that a careful selection of energy windows is essential for optimal imaging. Selection of Compton edges can be interesting as these may contain a sizeable number of counts as compared to the photopeaks.

2˙4.2. Usefulness of the ^{154}Eu gamma rays. The standard operation of the PGET device, using the 662 keV gamma ray, does not have sufficient capability of detecting missing fuel rods in the centre of the VVER-440 spent fuel assemblies from the Loviisa nuclear power plant [7]. In this respect, focusing on the 1274 keV gamma ray from ^{154}Eu may help as the attenuation coefficient of 1274 keV gamma rays in UO_2 is about half that of 662 keV gamma rays: 0.07 /mm vs. 0.16 /mm. The first results of such an investigation, using a 1200-1300 keV energy window, are reported in [6]. The conclusion is that the ^{154}Eu images are of similar quality to the ^{137}Cs images, but for a much smaller number of counts. This is a promising result: significantly increasing the data acquisition time for ^{154}Eu images may improve imaging of the centre of spent fuel assemblies. The same argument holds for larger fuel assemblies than those investigated in Finland, such as VVER-1000 and other PWR assemblies.

2˙5. *Recent developments*. –

2˙5.1. Serpent2 simulations. Monte Carlo simulations of radiation transport are very widely used in the development of instrumentation. If sufficiently realistic, they can be

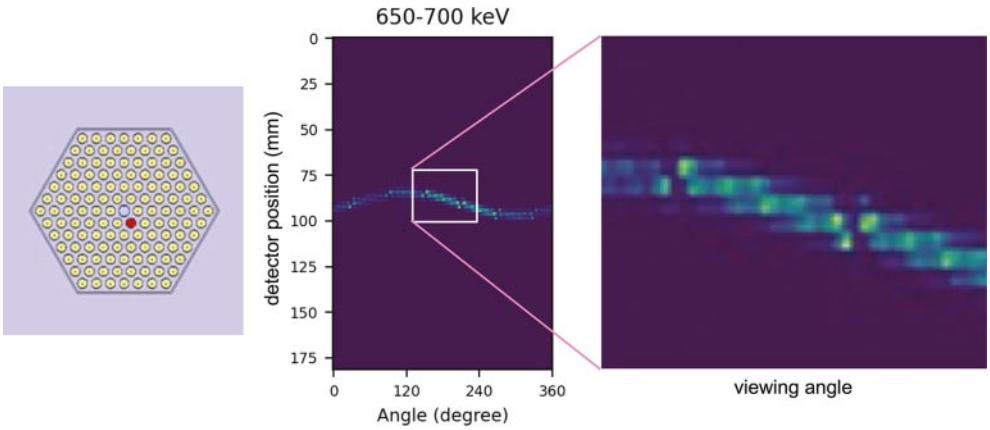

Fig. 4. – Results of a Serpent2 simulation considering a full VVER-440 fuel assembly, but with only 1 fuel rod, next to the central water hole, emitting gamma rays. The sketch of a VVER-440 assembly on the left highlights the emitting fuel rod. In the middle, the resulting sinogram is shown. The sinogram is the basic data obtained in a tomographic procedure: the number of counts versus detector position (1D spatial coordinate along the gamma camera) and viewing angle. The right image zooms in on part of the sinogram. See the text for more details.

used to make design decisions and to investigate situations that can not be (easily) measured. We have recently started using Serpent2 [9,10] to simulate PGET measurements in order to better understand the method. The technical drawing of the PGET instrument was imported into Serpent2. In order to reduce the calculation time, a variance reduction technique was implemented. We show here an example of the benefit of Monte Carlo simulations. Related to investigating imaging of the central part of a fuel assembly, it is interesting to investigate the contribution to the data from centrally located spent fuel rods. Figure 4 shows the results of a Serpent2 simulation considering a full VVER-440 fuel assembly, but with only 1 fuel rod, next to the central water hole, emitting gamma rays. The sinogram shows that at certain angles, when looking head-on at one of the corners of the assembly, no gamma rays are detected. This is due to strong absorption, because at this angle gamma rays have to travel through the centre of 5 fuel rods in order to reach the detector. Interestingly, the sinogram shows maximum count rates just next to the head-on angles, because these views provide a direct line of sight to the centre of the assembly. We are investigating, using both simulations and measurements, how this effect can be used to improve imaging of the centre of a fuel assembly. Some first measurement results are discussed in [6]. In order to better utilise this effect, the PGET device was recently modified to allow up to 720 angular bins, providing 0.5 degree steps.

2˙5.2. 3D position sensitive detectors. The PGET device has a small CZT semiconductor detector behind each collimator slit. Because of the small size, the probability that a gamma ray emitted from spent fuel (the 662 keV gamma ray from ^{137}Cs is the most important one) is fully absorbed is small. Full absorption is important as these photons provide the optimal imaging information. Detected events in which less than the full energy is detected may be related to photons that have Compton scattered before entering the detector (*e.g.*, inside the fuel, in the pond water or in the collimator) and thus have basically lost their imaging information. A larger fraction of full energy detec-

tion is possible using larger detectors. However, as the PGET collimators have a pitch of 4 mm, any such detector that is wider than 4 mm and thus covering more than one collimator slit, needs to have position sensitivity in order to know through which collimator slit a detected photon travelled. We have recently started to investigate the benefits of using state-of-the-art 3D position-sensitive semiconductor detectors (germanium and CZT) in PGET. The use of such detectors will increase the sensitivity, providing better images of weakly emitting objects and/or reducing the measurement time. The PGET collimators have a large vertical acceptance angle such that a roughly 30 cm long axial section of a fuel assembly is imaged at once. Better axial selection is possible by reducing the acceptance angle of the collimator, at the cost of smaller sensitivity and longer measurement times. However, using 3D position-sensitive detectors and the principle of Compton imaging, the vertical angle of the incoming gamma rays can be determined, providing detailed axial scanning with one measurement. In such a system, the excellent energy and spatial resolution of semiconductor detectors is essential. We have started the investigation of the use of 3D position sensitive detectors by Geant4 Monte Carlo simulations.

3. – Passive Neutron Albedo Reactivity (PNAR)

3˙1. *The PNAR principle.* – Figure 5 illustrates the principle of the PNAR method to investigate the presence of fissile material in a fuel assembly. Spent nuclear fuel naturally emits neutrons. If the fuel is surrounded by a neutron-moderating material, *e.g.*, the water of the spent fuel storage pool, the emitted neutrons will thermalise and some of them will enter the spent fuel assembly, the so-called neutron albedo. In case fissile material is present, these reflected neutrons will induce fission and thus cause extra neutrons to be emitted from the assembly. The amount of extra neutrons correlates with the amount of fissile material present. The PNAR method is based on the count rate of a fast neutron detector fairly close to the fuel assembly. The result of a PNAR investigation is the ratio of 2 measurements: the PNAR Ratio. In one measurement, the neutron albedo is left unmodified, resulting in the so-called high-multiplying situation. In the other measurement, the neutron albedo is strongly suppressed by a cadmium sheet that is introduced very close to the fuel assembly. The strong thermal neutron absorption of cadmium prevents thermal albedo neutrons from entering the fuel and inducing fission and extra neutrons. This is the low-multiplying situation. The final outcome, *i.e.*, the PNAR Ratio, is the neutron count rate in the high-multiplying situation divided by that in the low-multiplying situation.

3˙2. *The PNAR instrument design and operation.* – A PNAR instrument was designed based on extensive Monte Carlo simulations [11, 12]. The PNAR instrument for BWR fuel assemblies that was constructed and its operating characteristics are described in detail in [13, 14]. The instrument contains 4 detector pods arranged in a square tightly surrounding a BWR assembly which is lowered into the central opening. Each detector pod contains a fast neutron detector: a ^{3}He detector embedded in polyethylene covered by a thin layer of cadmium, making the detector sensitive to fast neutrons only. A xenon-filled ionisation chamber in each pod measures the total gamma radiation. A square cadmium liner is moved manually up to the level of the neutron detectors for the low-multiplying measurement and lowered to below the neutron detectors for the high-multiplying measurement. The cadmium liner is very close to the fuel assembly in order to maximise the PNAR Ratio and thus the sensitivity to the presence of fissile material.

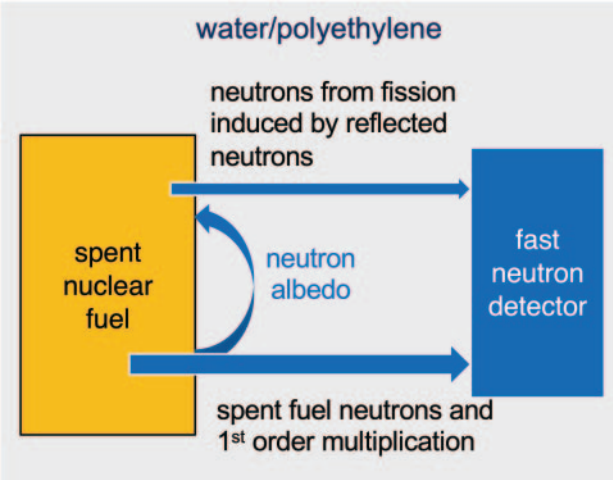

Fig. 5. – Illustration of the PNAR principle (see the text for a description).

3˙3. *A few results from PNAR measurements at the Finnish NPPs.* – A selection of PNAR Ratios are plotted as function of assembly burnup in fig. 6. All data points, except the one in the upper left corner of the graph, represent fully burnt assemblies. For such assemblies, the PNAR Ratio is similar, between about 1.04 and 1.05, due to the fact that the fissile material remaining in a fully burnt assembly is quite independent of the initial enrichment (IE). The data point in the upper left corner of the graph (low burnup and a large PNAR Ratio) is from a partially burnt assembly, therefore containing a relatively large amount of fissile material. From repeated measurements of a single assembly, the one standard deviation uncertainty of a PNAR Ratio measurement was determined to be 0.0013. An MCNP simulation shows a PNAR Ratio of 0.97 for a non-multiplying assembly. A fully burnt assembly thus has a PNAR Ratio that is about 50 standard deviations away from a non-multiplying assembly. This dynamic range is indicated in fig. 6.

4. – Combining PGET and PNAR

For measurements at the spent fuel storage pools, the PGET instrument is installed above the PNAR instrument, with the mid-planes of the instruments about 50 cm apart, see fig. 7. The same spent fuel assembly can thus be measured by both instruments at the same time, although at a slightly different axial position. Measurements at the same axial position can be performed in quick succession by lowering or raising the fuel assembly over about 50 cm. This enables to combine PGET and PNAR results, potentially providing useful extra information or confirmation of the results. We note that PGET and PNAR do not "see" the same axial part of a fuel assembly. The PGET axial field of view is determined by the collimator and is about 20 cm in the centre of the fuel assembly, whereas the PNAR measurement is sensitive to a fuel length of about 70 cm, determined by the length of the cadmium liner. An example of such a combination is shown in fig. 8. The PGET image shows a higher activity in the upper right corner than in the lower left corner. A higher activity indicates a higher burnup and thus a

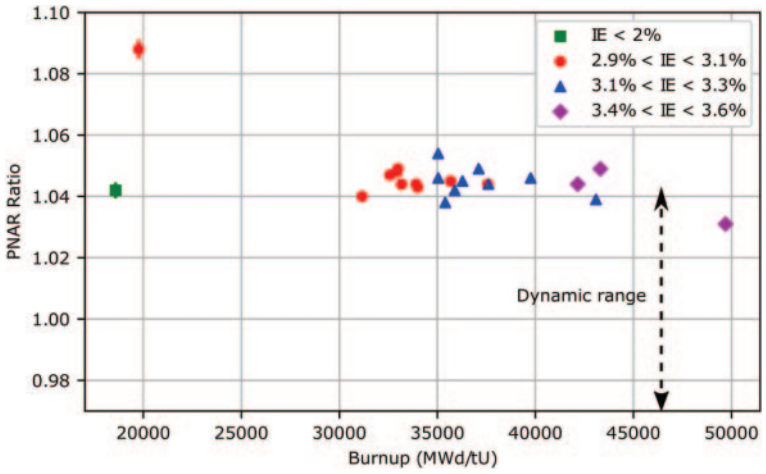

Fig. 6. – A selection of PNAR Ratios as function of assembly burnup. The symbol shape and colour relate to the fuel's initial enrichment (IE). Figure from [14]. See the text for a discussion of these results.

smaller amount of fissile material. As the PNAR Ratio is an indication of the amount of fissile material, it is anti-correlated with the activity: the PNAR Ratio's measured close to the higher, resp. lower, activity are lower, resp. higher. This result also shows that a PNAR Ratio measurement is more sensitive to the fuel rods that are closest to the neutron detector. This is the rationale behind having detectors all around the fuel assembly.

Fig. 7. – Left: the PGET and PNAR instrument at the top of their support structure before lowering into the spent fuel storage pool. Middle: A fuel assembly in measurement position. Right: Pool-side operation of the PGET and PNAR instruments.

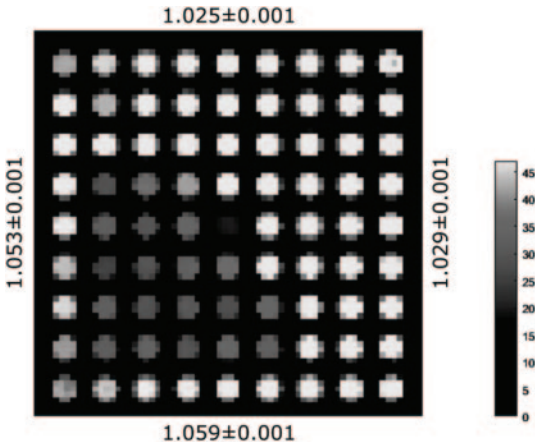

Fig. 8. – Combination of a PGET activity image and the PNAR Ratio's measured individually by the 4 neutron detectors for a 9×9-1 BWR assembly. The PGET image shows a higher activity in the upper right corner than in the lower left corner. The PNAR Ratios follow this trend, with a higher PNAR Ratio related to a lower activity. Figure from [14].

5. – Conclusions and outlook

Investigations over the last years have shown that PGET and PNAR measurements provide, for BWR fuel assemblies in the context of the Finnish geological repository, the comprehensive verification needed to assure that nuclear safeguards objectives are met and that all nuclear material stays in declared use. Such measurements are presently being implemented in preparation for the start of operations of the ONKALO repository, planned for 2025.

Research to improve the understanding and performance of the PGET and PNAR methods, and the value of combining their measurement results, continues. These efforts are supported by Monte Carlo simulations. We are also investigating whether fuel parameters and reactor history can be deduced from the measurements.

The development of new PGET and PNAR devices is being considered. Using relatively large 3D position sensitive semiconductor detectors for PGET has clear benefits. We are looking into quantitative PGET imaging, as well as PGET-like devices for imaging objects other than spent fuel assemblies. A PNAR instrument for the hexagonal VVER-440 fuel from the Loviisa nuclear power plant has been simulated [12, 15] and will be constructed in the future.

* * *

The authors wish to acknowledge CSC − IT Center for Science, Finland, for computational resources to perform the Serpent2 simulations.

REFERENCES

[1] `www.posiva.fi/en/index.html`.
[2] Dendooven P. and Bubba T. A., *Lect. Notes Phys.*, **1005** (2022) 245.

[3] Honkamaa T., Levai F., Turunen A., Berndt R., Vaccaro S. and Schwalbach P., in *Proceedings of the Symposium on International Safeguards, Vienna, Austria*, Paper IAEA-CN-220 (2014).
[4] White T., Mayorov M., Lebrun A., Peura P., Honkamaa T., Dahlberg J., Keubler J., Ivanov V. and Turunen A., *Proceedings of the 59th Annual Meeting of the Institute of Nuclear Materials Management; Baltimore, MD, USA* (2018).
[5] Mayorov M., White T., Lebrun A., Brutscher J., Keubler J., Birnbaum A., Ivanov V., Honkamaa T., Peura P. and Dahlberg J., *2017 IEEE Nuclear Science Symposium and Medical Imaging Conference* (IEEE) 2017.
[6] Virta R., Bubba T. A., Moring M., Siltanen S., Honkamaa T. and Dendooven P., *Sci. Rep.*, **12** (2022) 12473.
[7] Virta R., Backholm R., Bubba T. A., Helin T., Moring M., Siltanen S., Dendooven P. and Honkamaa T., *ESARDA Bull.*, **61** (2020) 10.
[8] Backholm R., Bubba T. A., Bélanger-Champagne C., Helin T., Dendooven P., and Siltanen S., *Inverse Probl. Imaging*, **14** (2020) 317.
[9] Leppänen J., Pusa M., Viitanen T., Valtavirta V. and Kaltiaisenaho T., *Ann. Nucl. Energy*, **82** (2015) 142.
[10] Kaltiaisenaho T., *Comput. Phys. Commun.*, **252** (2020) 107143.
[11] Tobin S. J., Peura P., Bélanger-Champagne C., Moring M., Dendooven P. and Honkamaa T., *ESARDA Bull.*, **56** (2018) 12.
[12] Tobin S. J., Peura P., Honkamaa T., Dendooven P., Moring M. and Bélanger-Champagne C., STUK Report (2018) `http://urn.fi/URN:ISBN:978-952-309-406-2`.
[13] Tupasela T., Master's Thesis, Aalto University (2019) `http://urn.fi/URN:NBN:fi:aalto-201908254886`.
[14] Tupasela T., Dendooven P., Tobin S. J., Litichevskyi V., Koponen P., Turunen A., Moring M. and Honkamaa T., *Nucl. Instrum. Methods Phys. Res. A*, **986** (2021) 164707.
[15] Tobin S. J., Peura P., Bélanger-Champagne C., Moring M., Dendooven P. and Honkamaa T., *Nucl. Instrum. Methods Phys. Res. A*, **897** (2018) 32.